Pergamon

European Journal of Cancer, Vol. 34, No. 9, pp. 1448–1454, 1998

Printed in Great Britain
0959-8049/98 $19.00+0.00

PII: S0959-8049(98)00195-6

Original Paper

Non-invasive *In Vivo* Mapping of Tumour Vascular and Interstitial Volume Fractions

R. Weissleder, H.C. Cheng, E. Marecos, K. Kwong and A. Bogdanov, Jr

Center for Molecular Imaging Research, Massachusetts General Hospital, 149 13th Street, Room 5403, Charlestown, Massachusetts 02129, U.S.A.

Non-invasive measurement of haemodynamic parameters and imaging of neovasculature architecture is of importance in determining tumour prognosis, in directing tissue sampling and in assessing treatment efficacy. In the current research we investigated a dual tracer nuclear magnetic resonance (NMR) technique to map the tumour vascular (VVF) and interstitial volume fraction (IVF) non-invasively *in vivo*. We hypothesised that a NMR signal emanating after intravenous administration of a vascular paramagnetic probe (MPEG-PL-GdDTPA) can be maximised so that additional signal after administration of a second interstitial probe (GdDTPA) would only reflect the IVF but not the VVF. The method and its assumptions were verified and experimental conditions optimised both in phantoms and in C6 glioma bearing rats. Data derived from *in vivo* studies show tumoral VVF and IVF values that are consistent with histology data and literature values; the relative ranking order of values was tumour > muscle > brain. Image maps showed intratumoral and intertumoral heterogeneity of both parameters at submillimetre pixel resolution. The method is applicable to a wide variety of tumour models and can theoretically be performed repeatedly to study tumour growth or involution during therapy. © **1998 Elsevier Science Ltd. All rights reserved.**

Key words: tumour, neovascularity, angiogenesis, vascular architecture, MR imaging
Eur J Cancer, Vol. 34, No. 9, pp. 1448–1454, 1998

INTRODUCTION

PREVIOUS RESEARCH has well established that tumour neovascularity is heterogeneous, both temporally and spatially [1] and that tumour vessels are often abnormally permeable to even large molecules and particles [2, 3], presumably because of the presence of highly permeable interendothelial junctions, transendothelial channels and discontinuous or absent basement membranes. The objective assessment of neovascular parameters is of prime biomedical interest both for predicting outcome [4–6] and assessing therapeutic efficacy of anti-angiogenic drugs. Morphological (diameter, density, architecture) and functional parameters (blood flow, vascular volume fraction, permeability, interstitial volume fraction) of tumour vasculature have been extensively studied in transparent chamber models [1, 7] or by injection of fluorescent dyes or polymers into tumour vessels followed by sacrifice of an experimental animal [1, 8, 9]. Although the first method allows intravital observation, results must interpreted cautiously [1] and may often not be applicable to tumours grown in anatomical locations not readily accessible to *in vivo* microscopy or in larger tumours.

Recent advances in nuclear magnetic resonance (NMR) imaging have led to the implementation of high resolution non-invasive imaging techniques that can be readily applied to tumour imaging. However, because image information is primarily dependent on local proton relaxation rates in a given tissue, the use of tracers is considerably more complex than with optical or other imaging techniques. Within the last few years different *in vivo* NMR techniques have been developed to measure tumoral vascular volume fraction (VVF) in animals, including fluorine NMR imaging of F19 fluorinated blood substitutes [10], fast NMR imaging after GdDTPA injection [11], or NMR imaging with macromolecular paramagnetic probes [12]. Many of these techniques are either not directly applicable to humans because of the unavailability of suitable vascular tracers or require extensive

Correspondence to R. Weissleder.
Received 6 May 1997; revised 8 Oct. 1997; accepted 10 Oct. 1997.

computational manipulation and ultrafast imaging to extract first pass kinetic principles.

We have established a simple method that allows 2 and 3 dimensional mapping of the tumour VVF and tumour interstitial volume fraction (IVF) independently during the same imaging session. The method is based on sequential injections of a large molecular weight (MW) paramagnetic marker (> 500 kDa) followed by a low MW (< 1 kDa) marker. Although VVF measurements after injection of the first probe are dose independent, we hypothesised that a high-dose can sufficiently decrease T1 relaxation time of blood so that the addition of a second, interstitial probe would allow additional estimation of IVF. The goal of the current study was to show the feasibility of the proposed method, determine tumoral heterogeneity of image maps and compare the obtained values to those published in the literature.

MATERIALS AND METHODS

Cell culture and tumour model

C6 rat glioma cells, a N-nitrosomethylurea-induced cell line obtained from the American Tissue Culture Collection (ATCC, CCL 107, Rockville, Maryland, U.S.A.), were cultured in Dulbecco's Modified Eagle Medium (DMEM) supplemented with 10% fetal bovine serum (FBS) (Cellgro, Mediatech, Washington, DC, U.S.A.) in standard tissue culture flasks (Falcon, Becton Dickinson, Lincoln Park, New Jersey, U.S.A.). The media was changed every 3 days. Prior to intracerebral stereotactic implantation, cells were mobilised from plates with a cell rake, counted and spun to a volume of 10 μL.

Female Fischer 344 rats ($n = 12$; Charles River Breeding Laboratories, Wilmington, Massachusetts, U.S.A.) weighing between 200 and 250 g were used for intracerebral implantation of C6 cells. Cells (10^6 cells in 10 μL) were stereotactically implanted into the right cerebral hemisphere. A linear skin incision was made over the bregma and a 1 mm burr hole was drilled into the skull approximately 0.5 mm posterior and 3.5 mm lateral to the bregma. A Hamilton 10-μl gas-tight syringe (Hamilton, Reno, Nevada, U.S.A.) was then used to inject 5 μl of the 9 L cell suspension (approximately 10^6 cells suspended in DMEM) into the putamen at a depth of 4 mm from the dural surface. The injection was made over 5 min and the needle was withdrawn slowly over another 5 min. The burr hole was occluded with bone wax (Ethicon, Inc., Somerville, New Jersey, U.S.A.) to prevent leakage of CSF and the skin was closed with a suture. The contralateral hemisphere was kept intact, so that it could serve as a normal control in each animal studied. The animal protocol was approved by the Institutional Review Committee on Animal Care and was conducted in accordance with national animal welfare guidelines.

Paramagnetic NMR probes

Two paramagnetic, gadolinium (Gd) containing probes were used: an intravascular probe and an interstitial probe. The intravascular probe was a methoxy polyethylene glycol (MPEG)-poly-L-lysine-Gd-DTPA graft copolymer [13]. Briefly, the agent consists of a central polylysine (PL, 36 kD average MW) chain to which were grafted protective methoxy poly (ethylene glycol) (MPEG, 5 kD average MW) side chains. One part of the poly-L-lysine aminogroups were modified with DTPA to yield $MPEG_{92}$-PL_{279}-$DTPA_{187}$, as confirmed by elemental analysis (calculated MW 560 kDa; Table 1). This agent has a systemic half-life in rodents of 36 h (human 20.6 ± 1.6 h) and shows virtually no leakage into tumours within the first 10 min after intravenous (i.v.) injection (time frame necessary for current experiments), however, after several hours, the agent does accumulate in tumour interstitium, similar to other long circulating macromolecular compounds because of high tumour vascular permeability and lack of lymphatic clearance from tumours [3]. The active drug compound, labelled with ^{99m}Tc, has also been tested in clinical trials [14] as an intravascular probe for human imaging applications. The drug compound had no measurable effect on cardiovascular parameters in rabbits or humans (A. Bogdanov, Massachusetts General Hospital, U.S.A.) or microvascular parameters in rats [15, 17]. The volume of distribution of this agents has previously been found to be similar to labelled red blood cells and human serum albumin [16, 17].

GdDTPA (0.538 KD) was obtained commercially (Berlex Laboratories, Wayne, New Jersey, U.S.A.) and its pharmacokinetic parameters have previously been determined in rodents: its systemic half-life is 10 min, its distribution volume is 0.2 L/kg, with 50% first pass extraction from vascular space (Table 1) [17, 18]. The distribution is thus similar to 51CrDTPA, commonly used as a marker of the interstitial volume space [19].

Theoretical considerations

Figure 1 summarises the theory underlying the model. The native NMR signal intensity of a spatially encoded voxel (grey box) reflects a variety of parameters such as proton density, relaxation times, flow, magnetic susceptibility, etc. The NMR signal originates from three distinct compartments in each voxel: the intravascular compartment, the interstitial compartment and the intracellular compartment. Following i.v. administration of paramagnetic vascular probe (which only reduces T1 relaxation time of blood; 'A' in Figure 1) the difference in signal intensity (ΔSI_A) in a given voxel reflects intravascular drug concentration and thus, VVF (Figure 2) [20]. The ΔSI_A can be maximised (i.e. by reducing T1 of blood to below 10 msec) after which additional i.v. administration of any paramagnetic probe does not further increase the signal intensity originating from the vascular compartment. If at this time, a second probe with high vascular/interstitium extraction coefficient is given ('B' in Figure 1), additional MR signal ΔSI_B will arise from T1 reduction of interstitial water (IVF). ΔSI_B thus correlates with the interstitial volume fraction while the slope of the curve reflects capillary permeability to GdDTPA (assuming a bolus injection).

Table 1. *Paramagnetic probes utilised*

Parameter	Vascular probe	Interstitial probe
Physicochemical		
Formula	$MPEG_{92}$-PL_{279}-$GdDTPA_{187}$	GdDTPA
MW	560 kDa	0.583 kDa
Size	10.3 ± 2 nm	< 3 nm
R1	18 $(mM\ sec)^{-1}$	4.1 $(mM\ sec)^{-1}$
Protein binding	None	None
Biological		
$T_{1/2}$ (rats)	36 h	10 min
Vd (rats)	0.04 L/kg	0.21 L/kg
Vascular extraction at first pass	Negligible	50%

Assumptions

Prior research has validated the use of macromolecular [12, 15, 17] and low molecular paramagnetic probes [11, 15, 17, 21, 22] for determining tumoral VVF [12], capillary permeability [21] and IVF, respectively, by using established markers such as labelled red blood cells or fluorescent dyes [10]. The theory underlying the current model builds on previously established techniques and uses the fundamentals of dual tracer kinetics in a multicompartment system [23]. During the first part of the study, a probe with an intravascular distribution is injected where $C(t) = G_0 \times e^{-Kt}(C(t)$ is the concentration of the probe at time t; Co is the plasma concentration after injection; K = elimination rate constant; and t is the time). During the second part of the study a probe with a distribution limited to the intravascular and interstitial space is injected with kinetics of an open two-compartment model. Several assumptions underlie the model and are discussed below.

Phamacokinetic parameters. The current model assumes that during the time of imaging (approximately 10 minutes for MPEG-PL-GdDTPA, and 5–10 min for GdDTPA) there is little variation in blood (MPEG-PL-GdDTPA) or tissue (GdDTPA) concentration of the probes during the measurement. The model also assumes relatively rapid (minutes) equilibrium between the vascular and interstitial space for GdDTPA (high extraction coefficient or permeability); this is reasonably well established for the majority of tumours [15, 17, 19, 22, 24] but is not necessarily the case for other tissues in which there exist diffusional barriers (e.g. brain and some brain tumours, testes). In addition, the method assumes no distribution of MPEG-PL-GdDTPA ('leakage') into tumour interstitium during the time of the study. The latter assumption is reasonable since tumoral accumulation of MPEG-PL-GdDTPA has previously been shown to require several hours (data not shown). The model also assumes that both tracers have the same initial vascular distribution during the two separate injections. Although tumour blood flow has been found to be heterogeneous, the temporal closeness between injections is expected to minimise different vascular distributions. Finally, the model assumes that no intracellular uptake of either probe occurs which is a likely assumption during the short imaging time.

Correlation between drug concentration and MR signal intensity. The NMR experiment does not directly measure the Gd concentration in tissue but rather measures the effect of Gd on proton relaxation times [25]. Using T1 weighted sequences, SI is directly proportional to T1 relaxation times of water protons in a given voxel [25]. The probes employed in this study have concentration dependent effects on relaxation times of water protons: at low tissue concentrations (< 3 μmol Gd/mL), the probes primarily decrease the longitudinal relaxation of water protons, visible as an increase in SI on T1 weighted images. At unphysiologically high concentrations (> 3 μmol Gd/mL), the probes also decrease the transverse relaxation of water protons, visible as a decrease in SI on T1 and T2 weighted images. Because of the complexity of this interplay and the differences in longitudinal relaxivity of both agents, a phantom study was initially undertaken to determine the ΔSI as a function of probe concentration (Figure 2); these data confirm that SI measurements predictably increase with concentrations up to approximately 3 μmol Gd/mL.

Water exchange. If a given water molecule that has been in close relation to a paramagnetic probe during a given time diffuses to a significant amount into another compartment during an imaging experiment, local drug concentration measurements will be inaccurate [26]. In order to minimise theoretical effects of such water exchange, we kept the repetition time (TR) low (14.1 msec). In addition, a previous study was not able to demonstrate fast transvascular water exchange in experimental tumours [17]. Because the current technique uses subtraction of voxels, effects related to water exchange may be further minimised, assuming that exchange rates are constant during signal acquisition.

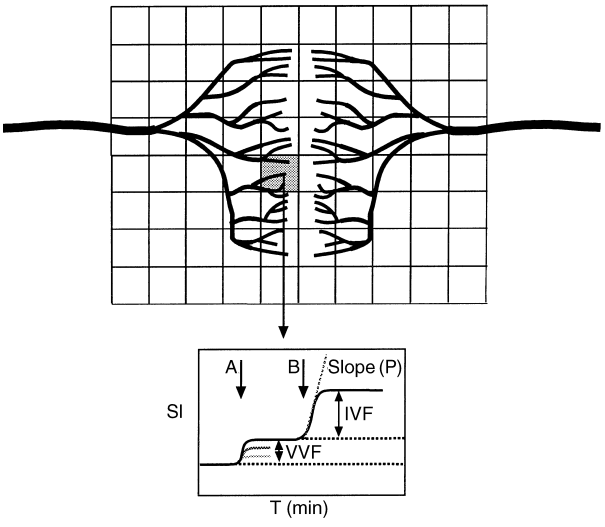

Figure 1. Model. Spatial encoding of tumour vasculature by NMR imaging allows sampling of small, submillimeter voxel sizes with conventional MR imaging systems. In a given voxel (grey shading) the change in signal intensity (SI) after injection of a vascular probe ('A') reflects the Gd concentration in the vascular space and correlates with VVF. Injection of a low MW second probe ('B') with a high vascular/interstitium extraction coefficient can then be used to estimate IVF. The technique is insensitive to blood flow because of the shortened T1 of the vascular compartment.

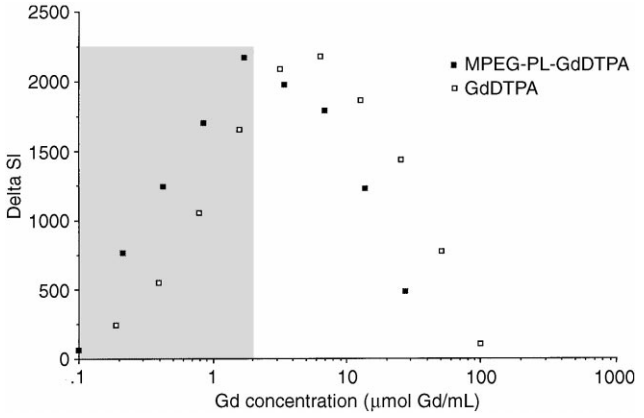

Figure 2. NMR SI of Gd containing phantoms. Changes in NMR signal intensity (delta SI) are plotted as a function of {Gd} for the two different paramagnetic probes (FSPGR 14.1/3.3/30°). The higher R1 relativity of the vascular probe (■) results in a left-shift of the curve when compared with the interstitial probe (□). The shaded grey area represents concentrations of Gd encountered *in vivo*.

Image analysis. In an effort to maximise the spatial resolution and signal-to-noise ratio (SNR) all imaging experiments were performed with surface coils where radiofrequency intensity (and thus, SI) decreases away from the center of the coil. Because of this field inhomogeneity external Gd phantoms were not used to estimate the true tissue Gd concentration. Rather, all measurements were made to internal standard tissue (striated muscle) at the same equidistant from the coil center as the tumour.

NMR imaging

NMR imaging was performed with a 1.5 T superconducting magnet (Signa 5.0; GE Medical Systems, Milwaukee, Wisconsin, U.S.A.) using a 3 in. surface coil, a field of view of 10 cm and a 128×256 matrix. The pulse sequence used consisted of an axial 3-D fast spoiled gradient recalled sequence (3-D-FSPGR) with a TR/TE/FA of 14.1/3.3/30°. This sequence was chosen because of its extreme T1 weighting, very short TR to minimize artifacts occurring from water exchange across the capillary wall and the presence of a spoiler gradient to minimise build-up of phase coherence in the transverse magnetisation [27]. The sequence was obtained repeatedly before and after injection of the imaging probes. During each 30 second acquisition a total of 12 contiguous 700 μm slices were collected.

Three different experiments were carried out. Initially, a phantom experiment was conducted to determine the effect of Gd concentrations of either probe on NMR SI since there exists a difference in relaxivity between the two agents. Secondly, experiments were carried out *in vivo* to determine whether increasing i.v. concentrations of the vascular probe would result in different VVF measurements. For this experiment 30 μmol Gd/kg aliquots of MPEG-PL-GdDTPA were injected during multiple acquisitions (total amount of agent injected was 90 μmol Gd/kg resulting in blood T1 relaxation times of < 50 msec [13, 28]. In the last set of experiments 90 μmol Gd/kg of MPEG-PL-GdDTPA was injected i.v. into tumour bearing animals since this dose was determined to be optimal from preceding experiments. The first injection was followed by i.v. injection of 200 μmol Gd/kg of GdDTPA (each injection being preceded by several series of acquisitions to establish steady state conditions). With the multiple acquisitions, the total scan time was approximately 20 min per animal. Following all imaging experiments, animals were sacrificed by an overdose of phenobarbital and brains were processed for histology.

Image analysis

All MR images were transferred to a Power Macintosh 7600 (Apple Computer, Cupertino, California, U.S.A.). Signal intensity measurements were subsequently measured in regions of interest (ROI) such as tumour, brain and striated muscle. Image analysis was performed by using NIH image 1.60/ppc (Rasband W., NIH, Bethesda, Maryland, U.S.A.) or other programs.

Average images were obtained from 3–5 images acquired in steady state prior to and following administration of imaging probes. Subtraction maps were acquired, in which average images were subtracted always using the raw image dataset. Pixel by pixel SI changes were calculated for ΔSI_{A-O} and ΔS_{B-A} correlating with VVF and IVF respectively (Figure 1). Since VVF and IVF of normal striated muscle are known, tumour tissue regions were scaled to muscle and expressed as the relative VVF (rVVF) and relative IVF (rIVF). Although true tumour VVF can be estimated by the same method by scaling SI to that of blood, such measurements are often technically difficult to obtain in small animals because of vessel misregistration due to motion or partial volume averaging. Data were also expressed as regions of interest drawn from brain and tumour regions of the maps.

Histology

Brains were removed and immersed in liquid nitrogen immediately after imaging. Crytome sections (Leica cryotome, Nussloch, Germany) of tumours were obtained at 8 μm thickness. The sections were fixed by cold ethylacetate/acetone/acetic acid (6:3:1) solution. Sections were then stained with haematoxylin eosin or Mason trichrome. Morphometric analysis of sections was performed to approximate the cellular and extracellular fractions. Sections were digitised with a charge coupled device (Photometrics, Tuscon, Arizona, U.S.A.) mounted on a Zeiss Axiovert 100 TV (Zeiss, Wetzlar, Germany) and connected to a Power Macintosh 7600/120). Image analysis was performed using commercially available segmentation software (ImageQuant, Molecular Devices, Sunnyvale, California, U.S.A.; IPLabSpectrum, Signal Analytics, Vienna, Virginia, U.S.A.).

Three tumour bearing animals also received an additional i.v. injection of biotin modified MPEG-PL-GdDTPA immediately after MR imaging to verify the intravascular distribution of the agent. The MPEG-PL precursor (30 mg, 10 mg/ml in 0.1 M Na carbonate, pH 8.7) was treated with 100 mg of 0'-biotinyl-PEG300-succinyl succinate for 2 h. After this, DTPA cyclic anhydride in DMSO was added at 5-fold molar excess over free amino groups and incubated for 4 h. The product was purified by extensive dialysis against 10 mM Na citrate, 0.15 M NaCl, pH 7. Brains of MPEG-PL-biotin DTPA injected animals were stained with the avidin-biotin complex kit (ABC kit, Vector Laboratories, Burlingame, California, U.S.A.) and sections were mildly counterstained with haematoxylin and eosin.

Statistical analysis

Quantitative results were analysed using the one tailed Student's *t* test. Statistical significance was assigned for *P* values of less than 0.05.

RESULTS

NMR signal intensity as a function of Gd concentration

Figure 2 shows the effect of the paramagnetic probes on NMR signal intensity of water. As predicted, low concentrations of either agent (< 2 μmol Gd/mL for MPEG-PL-GdDTPA and < 7 μmol/mL Gd for GdDTPA) increased the MR signal, whereas the highest concentrations tested decreased it. At Gd concentrations of up to 2 μmol Gd/mL experimental SI data and Gd concentrations were best fit by a binomial function where $C_{Gd} = \{-b +/- (b - 4ac)^{0.5}\}/2a$ with r^2 of 0.999 for either compound (for GdDTPA a = 71.5; b = 1413; and c = − 6.5; for MPEG-PLGdDTPA a = 2307; b = 3947; and c = 9.8). In a rough approximation and for the specific case of {Gd} < 0.4 μmol/mL data could also be fitted by a linear function with $C_{Gd} = SI/1355$ and $C_{Mpeg} = SI/1931$ (FSPGR 14.1/3.3/30°). The left shift of the latter curve reflects the higher R1 relaxivity of MPEG-PL-GdDTPA when compared to GdDTPA.

Dose response curve in vivo

Figure 3 summarises the effect of multiple sequential doses of MPEG-PL-Gd-DTPA on NMR SI in brain and muscle tissue. There was a stepwise increase in brain SI after each injection which saturated after three sequential doses of MPEG-PL-Gd-DTPA had been given (total of 90 μmol Gd/kg). These results are in accordance with phantom predictions in which SI peaked at approximately 2 μmol Gd/mL of MPEG-PL-GdDTPA (Figure 2). Assuming a rat weight of 200 g and 4% plasma volume, an i.v. injection dose of 90 μmol Gd/kg would result in an approximate plasma concentration of 2.2 μmol Gd/mL.

The rVVF (scaled to striated muscle) measurements of all brains studied during the multiple injections of MPEG-PL-GdDTPA were as follows: $rVVF_{30\,\mu mol}$ 0.93 ± 0.08; $rVVF_{60\,\mu mol}$ 0.90 ± 0.13; $rVVF_{90\,\mu mol}$ 0.91 ± 0.12; these data were not statistically significant from each other ($P > 0.5$) indicating that the measurements were dose independent. At saturation point the additional GdDTPA injection resulted in further increase of SI of striated muscle but not of brain parenchyma (Figure 3) as expected as GdDTPA readily crosses muscle capillaries but not an intact blood-brain barrier.

Tumour measurements

Figure 4 represents the temporal SI changes of different tissue compartments in a tumour bearing animal. As expected, the vascular SI increased to a maximum after injection of the first probe and did not significantly change after injection of the second probe (saturation). Brain tissue, likewise showed an initial increase in SI, with no further changes after the second injection (intact blood-brain barrier). Tumour and muscle showed two distinct plateaus of enhancement following injection of each probe. The absolute values of enhancement were higher for tumour than for muscle. The slopes of SI change were similar for tumour and muscle indicating similar permeability characteristics of these tissues.

SI measurements (mean ± S.D.) for the combined 12 tumour bearing animals ($n = 28$ slices analysed) showed a rVVF of tumours of 1.50 ± 0.67 (range: 0.5–2.12; values are relative to muscle). Assuming a true VVF of striated muscle of 5% the tumoral vascular space would be 7.5%/g tissue in this tumour model. The ranking of relative VVF for the tested tissues was: tumour > muscle ≥ brain. The relative IVF of tumour was 4.09 ± 1.16 (range 2.52–5.94; values are relative to muscle). Assuming a true IVF of striated muscle of 10% [29] the tumoral interstitial space would be 40%/g tissue in this tumour, similar to morphometric values obtained from histological sections ($37.2 \pm 7.7\%$) and similar to other published data [30].

When image maps were calculated to resolve spatially VVF and IVF at a submillimetre resolution (Figure 5) tumour heterogeneity became apparent. VVF maps generally showed a higher VVF in the tumour periphery than in the tumour centre and occasionally was asymmetric throughout the tumour (Figure 5). Tumours appeared more homogeneous on IVF maps but intratumoral and intertumoral heterogeneity was present.

Pathological examination of the specimen showed no evidence for tumoral necrosis or haemorrhage. Mean tumour volume was $66 \pm 10\,mm^3$. Histology confirmed that the distribution of MPEG-PL biotin DTPA was limited to the intravascular space without any evidence for interstitial accumulation in tumours 15 min after administration.

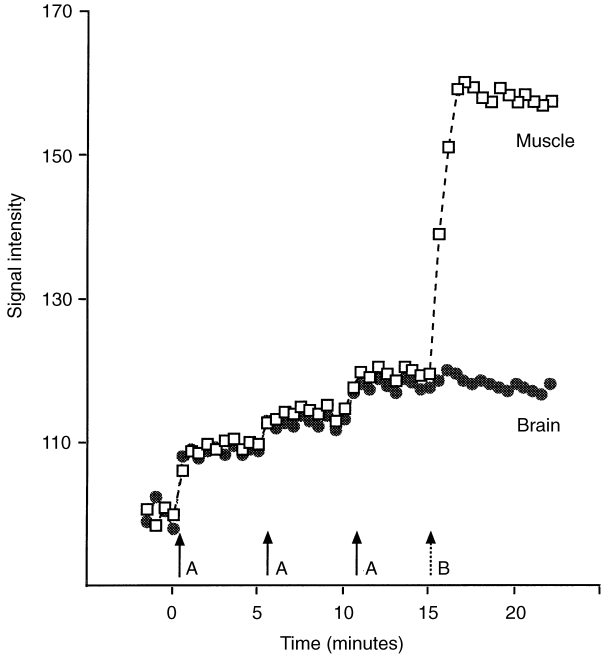

Figure 3. Dose response curve. Intravenous injection of 30 μmol Gd aliquots ('A') of the vascular probe show its effects on NMR SI of brain and muscle. Brain SI plateaued after a total of 90 μmol Gd injection. Intravenous injection of GdDTPA at this point ('B') does not further increase brain SI because of the intactness of the blood brain barrier but it significantly increased muscle SI because of leakage into the interstitium.

DISCUSSION

We have reported a technique to map tumour vascular and interstitial volume fractions *in vivo*. The results demonstrate the feasibility of the technique which utilises dual tracers and

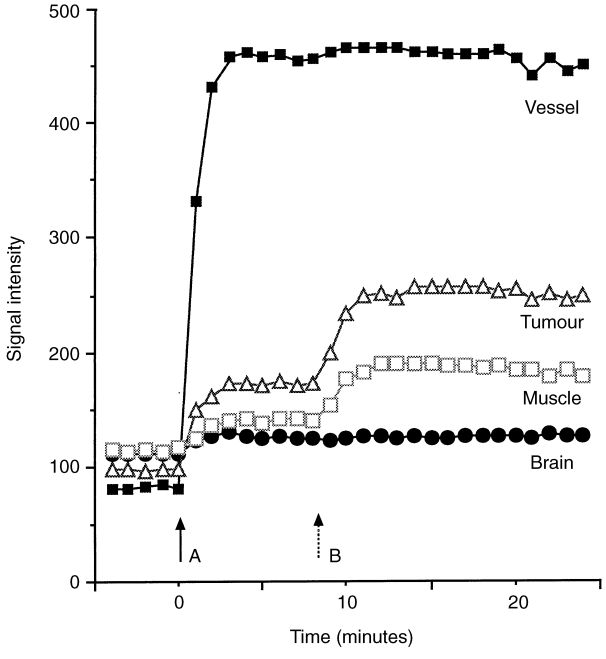

Figure 4. Brain tumour. Temporal SI measurements of different tissue compartments in a tumour bearing C6 animal. 'A' marks the i.v. injection of 90 μmol MPEG-PL-GdDTPA and 'B' marks the IV injection 200 μmol GdDTPA ('B').

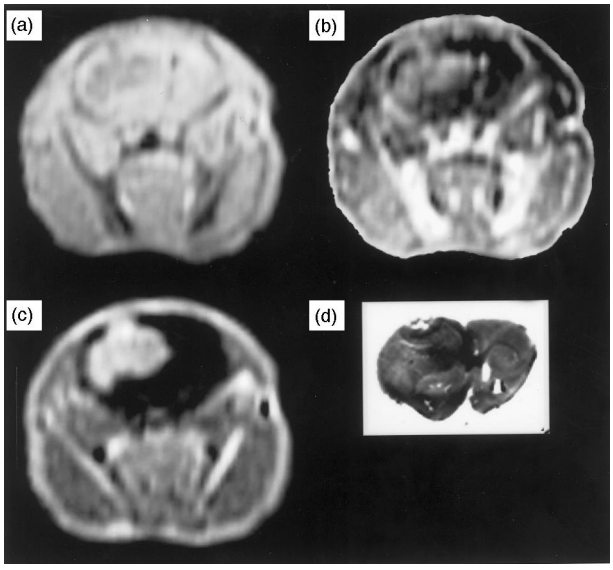

Figure 5. Regional VVF and IVF maps. (a) T1 weighted image at start of experiment shows the tumour to appear hypointense relative to surrounding brain. (b) VVF map where a high vascular volume fraction appears white (e.g. vessels, bone marrow) and areas of low VVF appear dark. (c) IVF map; except for brain (intact blood brain barrier), tissues with high interstitial volume fraction appear hyperintense. (d) H&E stain of corresponding section (magnification ×1.2).

MR imaging at high spatial resolution. The method is applicable to human tumours and should allow objective assessment of tumour vascular parameters which may have implications for diagnostic (prognosis, localisation of regions for biopsy) and therapeutic (antiangiogenesis therapy, chemotherapy, immunotherapy radiation therapy) purposes.

Tumour vascular volume fraction

The vascular space of tumours is highly variable temporarily and spatially and ranges from 1% in fibrosarcoma to 28% in lymphosarcoma [1]. The VVF measured with the current technique are in agreement with values found in the literature [10, 31]. The relationship of VVF to vascular 'hotspots' determined by histology is very interesting as the later are related to angiogenesis and metastasis [4–6] and to drug delivery to solid tumours [3, 32, 33]. Although it may appear intuitive that the VVF correlates with histologically determined microvascular density (using endothelial specific antibodies), previous studies have shown that the former are usually much lower than the latter [34]. For this reason, it will be important to develop neovascular probes with endothelial specificity in the future. Nevertheless, with the increasing number of anti-angiogenic and vascular targeting strategies undergoing clinical evaluation, VVF measurements may yet provide an important element in assessment of treatment efficacy.

Traditional methods of estimating VVF have mainly included micro-angiography or optical imaging techniques following injection of fluorescent dextrans or labelled RBC [1]. Several attempts have been made in the past to quantitate tumoral VVF and to calculate permeability surface area *in vivo* [11, 12, 21, 24, 35, 36]. These proposed methods often require ultrafast NMR imaging to capture first pass kinetics of rapidly leaking low MW agents and depend on certain assumptions of compartment models and exchange rates which may be highly variable [20, 37]. The current method is based on the recent availability of a NMR marker of the plasma volume [13], originally developed for MR angiography and imaging of cardiovascular function. Although other paramagnetic macromolecular markers have been used in the past to estimate VVF [12], development of those markers for clinical applications is unlikely. Most recently another vascular probe has become clinically available [38] and should be useable instead of the probe employed in the current study.

Vascular permeability and interstitial volume fraction

Extravasation of a molecule into tumour interstitium occurs mainly by convection (proportional to vascular/interstitial pressure difference) and diffusion (proportional to vascular/interstitial concentration difference). Tumour vascular permeability is one of the major factors which determines drug delivery to tumour interstitium and thus response of treatment [33, 39]. Since most chemotherapeutic agents have a relatively low MW in size (usually < 2 kD), the paramagnetic GdDTPA probe closely resembles such agents in MW [11, 40] and IVF studies may thus provide tissue distribution and uptake information. Measuring VVF, IVF and tumour volume will also allow the calculation of the tumour cellular volume fraction.

Tumoral heterogeneity

Results from this study showed a certain heterogeneity of VVF and IVF both within a given tumour, between tumours in different animals and also between themselves. VVF was typically highest in the tumour periphery, but not necessarily circumferential in a given tumour. WF was also heterogeneous within a tumour and between tumours. Interestingly, even direct comparison of slice matched VVF and IVF maps showed morphological heterogeneity (Figure 5). This discrepancy may be explained by several possibilities: (1) different types of microvascular networks within tumours have differing permeabilities to GdDTPA and MPEG-PL-GdDTPA; (2) there exist areas of stagnant blood flow and high interstitial tumour pressure; (3) temporal pressure differences between the two separate injections of the probe; and/or (4) presence of tumoral AV shunts. Irrespective of the precise underlying cause of tumoral heterogeneity, its presence underpins the importance of experimental probing if clinical decisions are based on tumour haemodynamic parameters. Since administration of each of the two paramagnetic probes resulted in different physiologic information it appears questionable whether the same information can be obtained by mathematical modeling of first pass kinetics previously performed with a single probe such as GdDTPA [11].

Clinical implications

The current study raises two questions regarding the clinical use of the method. The first is whether the measured haemodynamic parameters truly reflect tumour prognosis [4–6] and the second is whether the parameters can be effectively used to monitor, guide and triage patients to the most appropriate therapy. Although these answers await testing in a clinical setting, several studies have now confirmed an inverse relationship between tumour vascularity (determined as microvascular density in histological specimens) and patient survival [4–6]. Currently such determinations require tissue sampling and histological estimates which are subject

to spatial variability of the tumour sample. The currently proposed method would simplify such quantitation and be able to account for intratumour heterogeneity. It is thus not inconceivable that the method may be used for stratification of patients for anti-angiogenic or adjuvant therapy and to predict therapeutic response. We are currently testing the proposed method in a preclinical trial of anti-angiogenic peptides.

1. Jain R. Determinants of tumor blood flow; a review. *Cancer Res* 1988, **48**, 2641–2658.
2. Zou Y, Ling YH, Reddy S, Priebe W, Perez-Soler R. Effect of vesicle size and lipid composition on the in vivo tumor selectivity and toxicity of the non-cross-resistant anthracycline annamycin incorporated in liposomes. *Intern J Cancer* 1995, **61**, 666–671.
3. Yuan F, Dellian M, Fukumura D, *et al.* Vascular permeability in a human tumor xenograft: molecular size dependence and cutoff size. *Cancer Res* 1995, **55**, 3752–3756.
4. Weidner N, Semple JP, Welch WR, Folkman J. Tumor angiogenesis and metastasis-correlation in invasive breast carcinoma. *N Engl J Med* 1991, **324**, 1–8.
5. Weidner N, Folkman J, Pozza F, *et al.* Tumor angiogenesis: a new significant and independent prognostic indicator in early-stage breast carcinoma. *J Natl Canc Inst* 1992, **84**, 1875–1887.
6. Weidner N, Carroll PR, Flax J, Blumenfeld W, Folkman J. Tumor angiogenesis correlates with metastasis in invasive prostate carcinoma. *Am J Pathol* 1993, **143**, 401–409.
7. Hilmas D, Gillette E. Morphometric analysis of the microvasculature of tumors during growth and after irradiation. *Cancer* 1974, **33**, 103–110.
8. Jain R. Vascular and interstitial barriers to delivery of therapeutic agents in tumors. *Cancer and Metast Rev* 1990, **9**, 253–266.
9. Evelhoch JL. Measurement of tumor blood flow by deuterium NMR and the effects of modifiers. *NMR Biomedicine* 1992, **5**, 290–295.
10. Meyer K, Joseph P, Mukherji B, Livolsi V, Lin R. Measurement of vascular volume in experimental rat tumors by ^{19}F magnetic resonance imaging. *Invest Radiol* 1993, **28**, 710–719.
11. Su MY, Jao JC, Nalcioglu O. Measurement of vascular volume fraction and blood-tissue permeability constants with a pharmacokinetic model: studies in rat muscle tumors with dynamic Gd-DTPA enhanced MRI. *Magn Reson Med* 1994, **32**, 714–724.
12. Brasch R, Pham C, Shames D, *et al.* Assessing tumor angiogenesis using macromolecular MR imaging contrast media. *J Mag Res Imaging* 1997, **7**, 68–74.
13. Bogdanov AA, Weissleder R, Frank HW, *et al.* A new macromolecule as a contrast agent for MR angiography: preparation, properties, and animal studies. *Radiology* 1993, **187**, 701–706.
14. Callahan R, Bogdanov A, Fischman A, Brady T, Weissleder R. Pre-clinical evaluation and phase I clinical trial of a synthetic polymer contrast agent for blood pool imaging. *Am J Roent* 1998, in press.
15. Donahue KM, Weisskoff RM, Chesler D, *et al.* Improving MR quantification of regional blood volume with intravascular T1 contrast agents: accuracy, precision, and water exchange. *Magn Res Med* 1997, **36**, 859–867.
16. Callahan R, Wilkinson R, Bogdanov Jr. A, Donahue K, Weissleder R, Fischman A. Validation of plasma volume determinations in the rat using an In-111 labeled polymer and I-125 human serum albumin. *42nd Annual Meeting of the Society of Nuclear Medicine, Minneapolis, Minnesota*. Society of Nuclear Medicine, 1995, 157.
17. Donahue K, Weisskoff R, Parmelee D, *et al.* Dynamic Gd-DTPA enhanced MRI measurement of tissue cell volume fraction. *Magn Reson Med* 1995, **34**, 423–432.
18. Brasch R. Contrast-enhanced magnetic resonance imaging: why and how? In Brasch R, Drayer BP, Haughton VM, Jinkins JR, Nelson KL, Sze G, eds. *MRI contrast enhancement in the central nervous system*. New York, Raven Press, 1993, 1–10.
19. Reed R, Lepose S, Wiig H. Interstitial exclusion of albumin in rat dermis and subcutis in over- and dehydration. *Am J Physiol* 1989, **257**, H1819–H1827.
20. Roberts T. Physiologic measurements by contrast-enhanced MR imaging: expectations and limitations. *J Mag Res Imaging* 1997, **7**, 82–90.
21. Su MY, Najafi AA, Nalcioglu O. Regional comparison of tumor vascularity and permeability parameters measured by albumin-Gd-DTPA and Gd-DTPA. *Magn Reson Med* 1995, **34**, 402–411.
22. Kovar D, Lewis M, River J, Lipton M, Karczmar G. *In vivo* imaging of extraction fraction of low molecular weight MR contrast agents and perfusion rate in rodent tumors. *Magn Reson Med* 1997, **38**, 259–268.
23. Ritschel W. *Handbook of basic pharmacokinetics: including clinical applications, 3rd edition*. Drug Intelligence Publication Inc., Hamilton, Illinois, 1986.
24. Shames DM, Kuwatsuru R, Vexler V, Muhler A, Brasch RC. Measurement of capillary permeability to macromolecules by dynamic magnetic resonance imaging: a quantitative noninvasive technique. *Magn Reson Med* 1993, **29**, 616–622.
25. Buxton RB, Frank LR, Prasad PV. Principles of diffusion and perfusion MRI. In Edelman RR, ed. *Clinical Magnetic Resonance Imaging*. Philadelphia, WB Saunders, 1996, 233–270.
26. Kennan RP, Zhong J, Gore JC. On the relative importance of paramagnetic relaxation and diffusion-mediated susceptibility losses in tissues. *Magn Reson Med* 1991, **22**, 197–203.
27. Finn J, Simonetti O. Pulse sequence design in MRI. In Edelman RR, Hesselink JR, Zlatkin MB, eds. *Clinical Magnetic Resonance Imaging*. Philadelphia, WB Saunders, 1996, 145–176.
28. Hendrick RE, Haacke EM. Basic physics of MR contrast agents and maximization of image contrast. *J Mag Res Imaging* 1993, **3**, 137–148.
29. Aukland K, Reed R. Interstitial-lymphatic mechanisms in the control of extracellular fluid volume. *Physiological Reviews* 1993, **73**, 1–78.
30. Gullino P, Grantham F. The interstitial water space of tumors. *Canc Res* 1965, **25**, 727–731.
31. Fallowfield M. Vascular volume in B16 allografts and human melanoma xenografts estimated by means of Hoechst 33342. *J Pathol* 1989, **157**, 249–252.
32. Jain RK. Delivery of noval therapeutic agents in tumors: physiological barriers and strategies. *J Nat Cancer Inst* 1989, **81**, 570–576.
33. Yuan F, Salehi HA, Boucher Y, Vasthare US, Tuma RF, Jain RK. Vascular permeability and microcirculation of glioma and mammary carcinomas transplanted in rat and mouse cranial windows. *Cancer Res* 1994, **54**, 4564–4568.
34. Bernsen H, Rijken P, Oostendorp T, van der Kogel A. Vascularity and perfusion of human gliomas xenografted in the athymic nude mouse. *Br J Cancer* 1995, **71**, 721–726.
35. Tofts PS, Kermode AG. Measurement of the blood-brain barrier permeability and leakage space using dynamic MR imaging. 1. *Magn Reson Med* Fundamental concepts. 1991, **17**, 357–367.
36. Kuwatsuru R, Shames DM, Muhler A, *et al.* Quantification of tissue plasma volume in the rat by contrast-enhanced magnetic resonance imaging. *Magn Reson Med* 1993, **30**, 76–81.
37. Bauer WR, Hiller KH, Roder F, Rommedl E, Ertl G, Haase A. Magnetization exchange in capillaries by microcirculation affects diffusion-controlled spin-relaxation: a model which describes the effect of perfusion on relaxation enhancement by intravascular contrast agents. *Magn Reson Med* 1996, **35**, 43–55.
38. Mayo-Smith W, Saini S, Slater G, Kaufman J, Sharma P, Hahn P. MR contrast material for vascular enhancement: value of superparamagnetic iron oxide. *Am J Roent* 1996, **166**, 73–77.
39. Barnett PA, Roman-Goldstein A, Ramsey F, *et al.* Differential permeability and quantitative MR imaging of a human lung carcinoma brain xenograft in the nude rat. *Am J Pathol* 1995, **146**, 436–449.
40. Abramovitch R, Meir G, Neeman M. Neovascularization induced growth of implanted C6 glioma multicellular spheroids: magnetic resonance microimaging. *Cancer Res* 1995, **55**, 1956–1962.

Acknowledgements—We wish to thank R. Melder, Ph.D. for critically reviewing the manuscript and Carter Wright, for technical assistance. Supported in part from NIH 2RO1 CA54886-04A1 and 5RO1CA59649-03. H.C. Cheng was supported by the VGH-Taipei and National Yang-Ming University.